Free energy change for insertion of charged, monolayer-protected nanoparticles into lipid bilayers: Supplementary Information

Reid C. Van Lehn and Alfredo Alexander-Katz

1 Additional simulation details

In the main text, the total free energy change for translocating an AuNP from a solvated state to the center of a lipid bilayer is decomposed into a sum of several terms:

$$\Delta G_{total} = \Delta G_{phobic} + \Delta G_{insert} + \Delta E_{elec} + \Delta E_{thick} - T\Delta S_{conf} \quad (1)$$

The change in solvation free energy, ΔG_{phobic}, represents the primary hydrophobic driving force in the system. Physically, this term is related to both the enthalpic and entropic cost of exposing hydrophobic surface area to water, which reduces the number of hydrogen bonds in the system and forces surrounding water molecules into ordered, low entropy states[1]. Previous studies have shown that a simple approximation for the magnitude of this hydrophobic force is to scale the solvent-accessible surface area, or SASA, by a phenomenological proportionality constant, γ[2–4]. We thus simply write:

$$G_{phobic} = \gamma SASA \quad (2)$$

The SASA was calculated for each simulation timestep using the Shrake-Rupley "rolling ball" algorithm[5] using 100 uniformly distributed mesh points per hydrophobic bead and a probe size of 1.4 Å to represent water solvation. The SASA was only calculated for hydrophobic beads as free energy changes related to the hydrophilic beads are captured in the ΔG_{insert} term described below. The SASA reflects the unfavorable solvation of hydrophobic surface area by water, so the presence of the hydrophobic bilayer core and resulting decrease in solvent density in the core region decreases the SASA. To model the impact of the bilayer, a solvent density function, $\kappa(z)$, was defined as a function of the bilayer coupling parameter λ described in the main text. $\kappa(z)$ measures the effective solvent density at a distance z from the bilayer midplane ($z = 0$), where z is measured in nm. This function was approximated from molecular dynamics simulations of water in DOPC bilayers[6,7] as:

$$\kappa(z) = \begin{cases} 0.0 & z \leq 1.3\lambda \\ \dfrac{z - 1.3\lambda}{1.5\lambda} & 1.3\lambda < z \leq 2.8\lambda \\ 1.0 & z > 2.8\lambda \end{cases}$$

All numerical prefactors have units of nm so that $\kappa(z)$ is unitless. Recall that $\lambda = h/h_0$ is the perturbed thickness of the bilayer at the interface and is also unitless. A plot of $\kappa(z)$ for $\lambda = 1$ is shown in Fig. 2 of the main text.

The simple linear approximation scales the effective water density at the position z and we assume scales the SASA as well, providing a driving force for hydrophobic ligands to prefer the bilayer interior compared to full exposure to aqueous solvent. The total solvation free energy of the system as a function of λ is then written as:

$$G_{phobic} = \gamma \sum_{i}^{beads} \sum_{j}^{mesh} \kappa(z_{ij}) A_{ij} \quad (3)$$

The first sum runs over all hydrophobic beads in the system, while the second sum runs over all mesh points on that bead. For each mesh point, the SASA was incremented by an amount $\kappa(z_{ij})A_{ij}$ if the mesh point was not occluded by another bead in the simulation, where A_{ij} is the increment of the accessible surface area per point. The scaling factor κ_{ij} was only applied to ligands exposed to the bilayer, as many of the ligands would in principle be far from the bilayer region and thus would not be reasonably expected to be subject to a reduction in the SASA due to a change in the solvent density. Ligands were only marked as exposed if the number of solvent-accessible mesh points summed over all the beads in the ligand surpassed a threshold value and the location of the ligand was beyond a radial threshold from the AuNP center. Figure 2D in the main text provides a plot of the solvent density in the bilayer region. The total change in solvation free energy for a given value of λ was calculated by subtracting the value of G_{phobic} in the baseline state, where $\lambda = 0.0$ and $\kappa(z) = 1.0$ for all z. As discussed in the main text, we chose to test two different possible values of γ: 28 cal/mol/Å^2[8] and 47 cal/mol/Å^2[9]. As either parameter seems suitable for this work based on their derivations but their values differ considerably, the choice of this parameter is explored in the Results section of the main text.

The change in the free energy associated with exposing charged ligand end groups to the hydrophobic core of the bilayer is ΔG_{insert}. Previous implicit bilayer simulations have treated this term using a generalized Born model where the bilayer core is treated as a region of low dielectric constant and electrostatic contributions are calculated accordingly[10], or the bilayer is treated as a region of decreasing solvent density

based on comparison to simulations of protein side chain analogues[11]. We adopt a approach similar to the latter model and approximate the free energy penalty for insertion from free energy profiles for anion insertion into membranes[6,7]. The penalty resulting from this approach then takes into account free energy changes for observed behavior such as dragging water molecules into the bilayer environment, some lipid deformation, and any electrostatic effects. Furthermore, it directly accounts for any deviations in water density along the bilayer normal. The potential adopted is for a negatively charged side chain analogue in a DOPC bilayer[6], the closest approximation in the literature to the system studied here. The resulting potential is written as:

$$f(z) = \begin{cases} 20.32 - \dfrac{11.98z}{\lambda} & z \leq 1.0\lambda \\ 8.34 - \dfrac{6.36(z-1.0\lambda)}{\lambda} & 1.0\lambda < z \leq 1.75\lambda \\ 3.57 - \dfrac{3.40(z-1.75\lambda)}{\lambda} & 1.75\lambda < z \leq 2.80\lambda \\ 0.0 & z > 2.8\lambda \end{cases}$$

Here, $f(z)$ is the positive free energy change per ligand in kcal/mol as a function of z, the distance from the bilayer midplane ($z = 0$) in nm. The potential is scaled everywhere by λ to account for changes in the perturbed thickness of the bilayer. Only charged end groups on ligands marked as exposed to the bilayer, as described above, were subject to the penalty. Note that each charged end group was considered independently, although recent results suggest that the addition of multiple charged side chains leads to a non-additive energy barrier[12]. However, here we assume that due to the symmetry of the spherical AuNP core the bilayer will tend to deform in a uniform manner to limit charge exposure as captured by the ΔE_{thick} term, effectively taking into account any cooperative effects. We thus assume that the resulting charge penalty can be treated for each end group independently. Figure 2D in the main text shows a plot of this potential for a value of $\lambda = 1.0$.

While ΔG_{insert} accounts for electrostatic interactions between charged end-groups and the bilayer, ΔE_{elec} accounts for electrostatic interactions between charged end-groups with each other. Recent studies have shown that the electrostatic potential near the surface of charged monolayer-protected AuNPs can be well-described by Debye-Hückel theory, which we assume here as well[13–15]. The electrostatic energy between ligands is then calculated via a screened Coulomb pair potential of the form:

$$\psi(r) = \frac{Q}{4\pi\varepsilon r} e^{-r/\lambda_D} \tag{4}$$

Here, λ_D is the Debye length of the system. All simulations used a Debye length of 0.8 nm corresponding to a physiological salt concentration of 0.150 mM. The dielectric constant was set to 80 for all interactions due to the presence of aqueous solvent. To account for the bilayer, the potential between charges on opposite sides of the bilayer was set to 0 to match the results of numerical solutions to the non-linear Poisson-Boltzmann equation near membrane surfaces[16,17]. All ligand end groups were assumed to be charged with no possibility for charge regulation due to the pKa of sulfonate, which has been measured as approximately -2.8. Based on these assumptions, the total electrostatic energy in the system is given by:

$$E_{elec} = -1.0e \sum_i \sum_{j>i} \psi(|r_i - r_j|) \tag{5}$$

The final energetic component is the penalty for bilayer thickness deformations around the embedded AuNP. By varying the value of λ, the bilayer was able to adjust its thickness to match the particle, a process referred to as *hydrophobic matching* in studies of bilayer-protein interactions[18]. To penalize thickness deformations away from the equilibrium bilayer thickness, we utilize a phenomenological spring model that has been previously parameterized to the mechanical properties of known lipids[19,20]. For DOPC, the deformation energy in kcal/mol is:

$$\Delta E_{thick} = 202.5(\lambda - 1.0)^2 R^{0.815} \tag{6}$$

Here, R is the radius of a cylindrical inclusion that is calculated from the average radius of the particle and monolayer in the x-y plane. The bilayer thickness penalty is strictly a function of λ and thus is not calculated during simulations, but rather is added to the total system free energy calculated for each value of λ based on the average value of R calculated during simulations.

1.1 Free energy calculations using BAR

A major contribution to the total free energy change of insertion is the change in the conformational entropy of the monolayer ligands. In the baseline state, the ligands are relatively free to explore the spherical volume around the AuNP surface; however, in the embedded state, the significant penalty associated with the insertion of charged residues reduces the conformational freedom of end-functionalized ligands. To capture this change in conformational entropy, ΔS_{conf}, we calculate the total system free energy change using the Bennett Acceptance Ratio (BAR) method[21,22]. BAR requires the definition of two thermodynamic states with distinct potential energy functions such that the energy of a given system configuration can be calculated for either state. Configurations are then generated separately for each state according to its potential energy function, but the energy of each configuration calculated using both states' potential energy functions is saved. The total free energy change is then calculated by the relation:

$$\Delta G_{0\to 1} = kT\left[\ln\frac{\Sigma_1 f(U_0-U_1+C)}{\Sigma_0 f(U_1-U_0-C)}\right]+C \tag{7}$$

Here, Σ_0 represents a sum over configurations generated with the potential energy function corresponding to state 0, U_0 is the potential energy of each configuration calculated with potential energy function for state 0, U_1 is the potential energy of each configuration calculated with the potential energy function for state 1, $f(x)$ is the Fermi function, and C is a constant. The Fermi function is defined as:

$$f(x) = \frac{1}{1+e^{x/kT}} \tag{8}$$

The constant C is defined as:

$$C = kT\ln\frac{Q_0}{Q_1} \tag{9}$$

Here, Q_0 and Q_1 are the partition functions of states 0 and 1 respectively, so solving for the constant C is equivalent to finding the free energy change between the two states. C is determined by iteratively solving the equation:

$$\sum_1 f(U_0-U_1+C) = \sum_0 f(U_1-U_0-C) \tag{10}$$

Comparing eq. 7 and eq. 10 confirms that the value of C that satisfies eq. 10 is the free energy change between state 1 and 0. The BAR algorithm thus consists of first running simulations to generate configurations for both states 0 and 1, saving the energy of each configuration calculated using the energy functions of both states, then self-consistently solving eq. 10 to determine the free energy change after all configurations are generated.

In this system, a thermodynamic state is defined by choosing a value of λ corresponding to a particular bilayer thickness. The free energy change between state 0 with $\lambda = \lambda_0$ and state 1 with $\lambda = \lambda_1$ is equivalent to the free energy change associated with increasing the perturbed bilayer thickness around the embedded AuNP. Setting a value of $\lambda = 0.0$ is equivalent to the particle in a completely solvated state with no bilayer, which defines the reference state for all free energy changes. For each simulation run, 15 values of the λ parameter were attempted, incrementing from an initial value of $\lambda = 0.0$ to a maximum value of $\lambda = 1.2$. For each value of λ tested, the simulation was first equilibration for 50,000 Monte Carlo timesteps per bead in the system, then configurations were recorded for 100,000 Monte Carlo timesteps per bead. Every 20 timesteps the energy of the system was calculated for both the current and next value of λ and these energies were saved for later input to Eq. (10). These values were sufficient to obtain convergence via the BAR algorithm. The global free energy minimum for a particular simulation as a function λ was estimated by using a quadratic interpolation between the intermediate values of λ tested[23].

2 Grid point analysis of AuNP conformations

To gain a more accurate picture of the conformational state of the AuNPs before and after insertion, Figure S1 shows the average occupancy of all beads of the AuNP (top row) and average occupancy of just the hydrophilic beads (bottom row) of a 2.5 nm diameter, 1:1 MUS:OT mixed AuNP in the solvated (left) and inserted (right) states. The average occupancy is calculated by dividing the simulation box into cubic grid with a grid separation of 0.1 nm. For each simulation configuration, each bead in the system is checked to see if it occludes grid points, in which case a counter for that grid point and bead type is incremented. The graphs show the average of these counters over all simulation timesteps and further averaged by rotating around the normal to the membrane to yield a two-dimensional representation of spatial occupancy. The results show that in the baseline state all beads, including hydrophilic beads, are effectively able to explore the full conformational landscape around the AuNP, as would be expected in the absence of a bilayer perturbing the ligand conformations. In contrast, upon insertion, the ligand conformations and thus average occupancies are biased toward the bilayer interface. The top right plot in Figure S1 shows the interesting result that the actual interface of the monolayer with the bilayer core region appears almost planar given the preference of hydrophobic ligands for the core region. This observation implies that the embedded AuNP could strongly resemble a transmembrane protein. The bottom right plot shows that on average hydrophilic beads strongly prefer the bilayer-solvent interface, as expected due to the prevalence of ligand snorkeling.

3 Clustering of ligands in baseline state

The clustering of monolayer ligands in the baseline state as shown in Figure 3 of the main text is driven by the decrease in the hydrophobic surface area. The extent of clustering is thus a function of γ, as described in the Simulation Methods. Figure S2 shows the free energy change associated with changing γ from an initial value of 0 to 60 cal/mol/Å^2 for a 2.5 nm 2:1 MUS:OT particle.. The free energy change is decomposed into both a component calculated from the SASA, ΔG_{phobic}, and an entropic component calculated using the BAR methodology, $-T\Delta S_{conf}$. The increase in the SASA parameter drives the increase in ΔG_{phobic} as expected. The entropic free energy also increases, reflecting the greater drive for ligands to cluster as the SASA parameter becomes stronger, reducing the number of low energy configurations in the system. The tendency

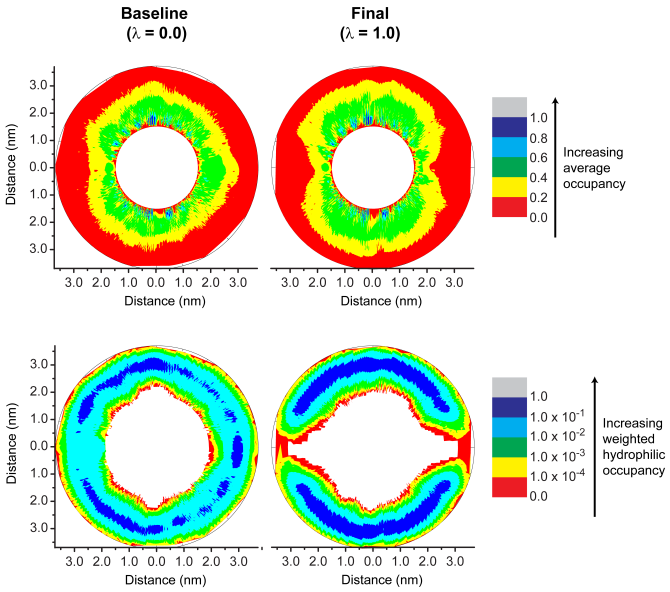

Fig. S1 Representation of average spatial occupancy by all ligand beads (top row) and just hydrophilic beads (bottom row) for the baseline and embedded states. The average occupancy was calculated using a cubic grid as described in the text. Results are shown for a 2.5 nm diameter 1:1 MUS:OT AuNP.

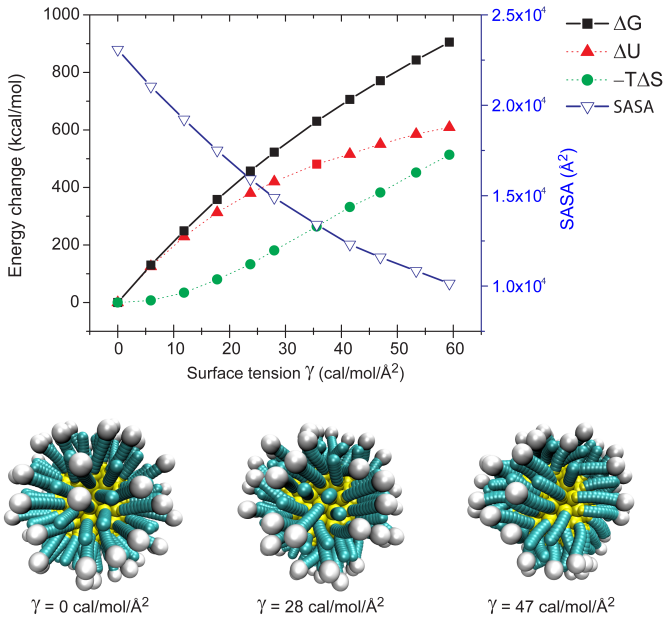

Fig. S2 Free energy change for increasing the SASA parameter γ from an initial value of 0.0, representing no penalty for solvent exposure, for a 2.5 nm 2:1 MUS:OT particle. The free energy change is decomposed into a hydrophobic term calculated by multiplying the exposed hydrophobic surface area by γ and an entropic term related to the reduction in the conformational entropy of the ligands. As γ is increased, both the enthalpic and entropic free energy terms increase. The increase in the entropic component is explained by the tendency of ligands to cluster to minimize exposed surface area as shown by the decrease of the SASA with increasing γ. The simulation snapshots are averaged over several configurations to show the increased tendency for clustering at larger γ values.

to cluster is further illustrated by the actual decrease of the amount of SASA as shown in the blue curve with open symbols. The simulation snapshots in Figure S2 show average ligand positions over the simulations corresponding to the γ values listed. Consistent with the free energy results, clustering is more apparent for larger values of the SASA parameter. The two positive values of the SASA parameter shown correspond to the two experimental values described in the Methods section. On the basis of these observations, it is apparent that this implicit solvent methodology is able to reproduce the ligand clustering observed in previous molecular dynamics simulations [24,25] at a fraction of the computational cost, with γ acting as a primary tuning parameter in the system.

References

1 D. Chandler, *Nature*, 2005, **437**, 640.
2 C. Chothia, *Nature*, 1974, **248**, 338.
3 T. Ooi, M. Oobatake, G. Némethy and H. A. Scheraga, *Proc. Natl. Aca. Sci. USA*, 1987, **84**, 3086.
4 J. R. Livingstone, R. S. Spolar and M. T. Record, *Biochemistry*, 1991, **30**, 4237.
5 A. Shrake and J. Rupley, *J. Mol. Biol.*, 1973, **79**, 351.
6 J. L. MacCallum, W. F. D. Bennett and D. P. Tieleman, *J. Gen. Physiol.*, 2007, **129**, 371.
7 J. L. MacCallum, W. F. D. Bennett and D. P. Tieleman, *Biophys. J.*, 2008, **94**, 3393.
8 D. Sitkoff, N. Ben-Tal and B. Honig, *J. Phys. Chem.*, 1996, **100**, 2744.
9 K. A. Sharp, A. Nicholls, R. F. Fine and B. Honig, *Science*, 1991, **252**, 106.
10 M. Feig and C. L. Brooks III, *Curr. Opin. Struct. Biol.*, 2004, **14**, 217.
11 M. B. Ulmschneider, J. P. Ulmschneider, M. S. P. Sansom and A. Di Nola, *Biophys. J.*, 2007, **92**, 2338.
12 J. L. MacCallum, W. F. D. Bennett and D. P. Tieleman, *Biophys. J.*, 2011, **101**, 110–117.
13 P. Guo, R. Sknepnek and M. Olvera de la Cruz, *J. Phys. Chem. C*, 2011, **115**, 6484.
14 E. Heikkilä, A. A. Gurtovenko, H. Martinez-Seara, H. Häkkinen, I. Vattulainen and J. Akola, *J. Phys. Chem. C.*, 2012, **116**, 9805.
15 M. J. Zimmer and T. Geyer, *J. Chem. Phys.*, 2012, **136**, 125102.
16 K. E. Forsten, R. E. Kozack, D. A. Lauffenburger and S. Subramaniam, *J. Phys. Chem.*, 1994, **98**, 5580.
17 V. B. Arakelian, D. Walther and E. Donath, *Colloid Polym. Sci.*, 1993, **271**, 268.
18 M. O. Jensen and O. G. Mouritsen, *Biochim. Biophys. Acta*, 2004, **1666**, 205.
19 C. Nielsen, M. Goulian and O. S. Andersen, *Biophys. J.*, 1998, **74**, 1966.
20 C. Nielsen and O. S. Andersen, *Biophys. J.*, 2000, **79**, 2583.
21 C. H. Bennett, *J. Comput. Phys.*, 1976, **22**, 245.
22 G. König, S. Bruckner and S. Boresch, *J. Comput. Chem.*, 2009, **30**, 1712.

23 W. H. Press, S. A. Teukolsky, W. T. Vetterling and B. P. Flannery, *Numerical Recipes in C (2nd ed.): The Art of Scientific Computing*, Cambridge University Press, New York, NY, USA, 1992.

24 P. K. Ghorai and S. C. Glotzer, *J. Phys. Chem. C.*, 2007, **111**, 15857.

25 J. M. D. Lane and G. S. Grest, *Phys. Rev. Lett.*, 2010, **104**, 235501.